ELSEVIER

Journal of Power Sources 94 (2001) 20–25

JOURNAL OF POWER SOURCES

www.elsevier.com/locate/jpowsour

Performance of a solid oxide fuel cell utilizing hydrogen sulfide as fuel

M. Liu, , P. He, J.L. Luo*, A.R. Sanger, K.T. Chuang

Department of Chemical and Materials Engineering, University of Alberta, Edmonton, AB, Canada T6G 2G6

Received 20 September 2000; accepted 1 October 2000

Abstract

The electrochemical performance of a hydrogen sulfide solid oxide fuel cell having the configuration H_2S, Pt/$(ZrO_2)_{0.92}(Y_2O_3)_{0.08}$/Pt, air has been examined at atmospheric pressure and 750–800°C, using both pure and 5% H_2S anode feed streams. The performance of the cell is higher when using diluted H_2S feed compared with pure H_2S feed: current densities up to 100 mA cm^{-2} and power densities up to 15.4 mW cm^{-2} have been achieved using diluted H_2S gas (5%) at 800°C. However, the platinum anode degrades over time in H_2S stream due to the formation of PtS. Electrochemical oxidation of H_2S on the Pt anode significantly accelerated its degradation. Polarization and impedance spectroscopy measurements show that at low current density (*i*) electrochemical reaction is the major cause of polarization in the fuel cell. Ohmic loss due to the resistance of the electrolyte material and the electrical connecting wire is a major part of cell polarization at high *i*.

Keywords: Solid oxide fuel cell; Hydrogen sulfide; Platinum electrode; YSZ

1. Introduction

In recent years, solid oxide fuel cells (SOFCs) using hydrogen as fuel have been investigated extensively, and may soon provide a viable commercial option for power generation [1]. Hydrogen sulfide is also a good candidate as a fuel for SOFCs. H_2S has a high chemical potential (0.742 V if sulfur is produced and 0.758 V for SO_2 as the product, at 750°C and 1 atm). However, much less effort has been made in the development of H_2S–O_2 fuel cells compared with H_2–O_2 fuel cells [2–6]. A major factor is that H_2S is an extremely corrosive and noxious gas, which puts stringent requirements on cell materials, especially at high temperatures. H_2S currently is removed from gas streams using absorption processes [7,8]. H_2S gas is partially oxidized to elemental sulfur and water vapor via the well-established Claus process. The reaction is highly exothermic. Thermal energy can be recovered as low-grade energy in the steam produced. However, it is much more desirable to recover this energy as electricity in a highly efficient manner.

The feasibility for electrochemically oxidizing H_2S in a fuel cell was first demonstrated in the late 1980s. Pujare et al. showed that a solid oxide fuel cell based on yttria-stabilized zirconia (YSZ) electrolyte could operate on high levels of H_2S fuel at 900°C [2]. Subsequent studies by the same group revealed that various thiospinels and metal sulfides were active as anode electrocatalysts for H_2S oxidation [3]. The potential for utilization of H_2S in ceria-based solid electrolyte cells with porous platinum electrodes has also been demonstrated [4,5]. However, while doped ceria exhibits higher ionic conductivity than YSZ, the electronic conductivity of ceria in a reducing atmosphere reduces the open circuit potential [5,9]. Much improved H_2S–O_2 fuel cell performance was achieved recently using thinner YSZ electrolytes (thickness between 40 and 500 μm) and new active anode materials ($Li_2S/CoS_{1.035}$ and WS_2) with low overpotentials [6]. State of the art YSZ is the favored electrolyte material, due to its relatively high ionic conductivity and high chemical stability. Alternative available oxide ion conductive membranes deteriorate over time on stream or have other unfavorable performance characteristics [9]. The ability of Pt to electrochemically catalyze the oxidation of H_2S at temperatures above 650°C has been demonstrated [5,10]. Herein we will describe use of H_2S as anode fuel in laboratory scale SOFCs having YSZ electrolytes and Pt electrodes, at 1 atm and 750–800°C. We will show that deterioration of Pt anodes is caused by reversible formation of PtS, and identify the contributing factors to ohmic resistance in the cell.

* Corresponding author. Tel.: +1-780-492-2232; fax: +1-780-492-2881.
E-mail address: jingli.luo@ualberta.ca (J.L. Luo).

0378-7753/01/$ – see front matter
PII: S0378-7753(00)00660-1

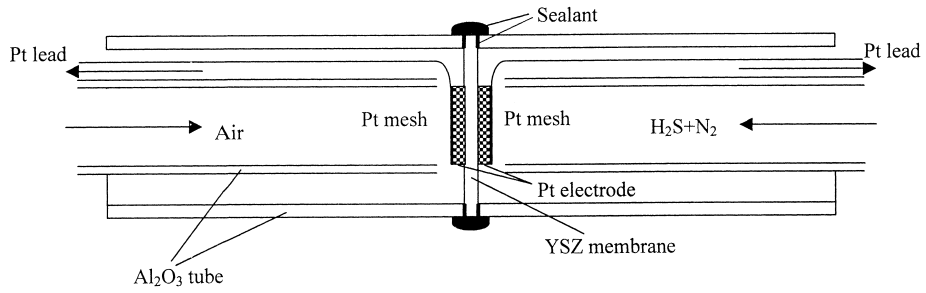

Fig. 1. Fuel cell assembly.

2. Experimental

2.1. Cell design

A schematic diagram of a two-compartment planar cell geometry is shown in Fig. 1. The cell comprises a membrane electrode assembly (MEA) having anode and cathode compartments sealed to the respective faces of the MEA.

Tape casted 8 mol% YSZ disks with a thickness of 0.2 mm and a diameter of 2.54 cm were used as electrolytes. Both cathode and anode catalysts were platinum, prepared by screen printing platinum paste (Heraeus CL11-5100) onto the anode and cathode surfaces of the YSZ electrolyte. After drying in the atmosphere for 3 h, the paste was further dried at 130°C for 10 min and then fired at 1050°C for 30 min to form porous electrodes. The superficial surface area of each electrode was approximately 1 cm^2. Platinum gauze (52 mesh) was used as the current collector for both anode and cathode. A platinum lead wire was spot-welded to each current collector. The total wire length was ca. 1 m. The MEA was sandwiched between the outer tubes of the anode and cathode compartments. The outer perimeter of each outer tube was sealed to the MEA by applying a thin layer of ceramic adhesive (Aremco 503).

The anode and cathode compartments each comprise two co-axial alumina tubes. The inner tube extends from outside the heated reaction zone to a position close to each electrode of the MEA. The two tubes are sealed together at the remote end, except for a spent gas outlet. After the anode and cathode compartments had been sealed to the MEA, the assembled cell was placed in a tubular furnace (Thermolyne F79300) having a uniform temperature zone: ±0.6°C over the central 7.62 cm length of the cell and ±3.0°C to distances up to 7.62 cm each side of the MEA. The seals were cured as the cell was heated to the prescribed temperature for testing, prior to operation of the cell under reaction conditions. The fuel cell assembly then was leak tested.

Experiments were conducted in the temperature range 750–800°C. Fuel gas mixture comprising either 5% H_2S balanced with nitrogen or pure H_2S was introduced into the anode compartment via the inner tube. Spent gas exited the anode compartment via the gas outlet in the outer tube. Air was supplied to the cathode surface via the inner tube of the cathode compartment. Spent air exited the cathode compartment via the gas outlet in the outer tube.

2.2. Electrochemical apparatus

The open circuit voltage between anode and cathode was monitored using a Keithley 199 digital multimeter. Potentiodynamic current-potential measurements were performed using a Pine AFRED5 potentiostat/galvanostat operating in potentiostat mode in conjunction with a VirtualBench data acquisition system. Cell electrochemical impedance analysis was carried out using a Gamry CMS 100/300 impedance measurement system combined with a Stanford SR810 DSP Lock-in amplifier under open-circuit voltage (OCV) and polarization conditions. Impedance data typically were obtained over the frequency range 50 kHz to 1 Hz.

3. Results and discussion

3.1. Open circuit voltage (OCV) of the H_2S–O_2 fuel cell

The open circuit voltage of the H_2S–O_2 fuel cell using 5% H_2S as anode feed and air as cathode feed at 750 and 800°C was 1.07 and 1.11 V, respectively. The calculated values (ΔE^0) based on thermodynamic data ($\Delta G^0(T)$, HSC Chemistry Software, Version 1.12, Outokumpu Research) for H_2S oxidation to either sulfur or SO_2 are: 0.742 V at 750°C and 0.726 V at 800°C for reaction (1), and 0.758 V at 750°C and 0.750 V at 800°C for reaction (2).

$$H_2S(g) + \tfrac{1}{2}O_2(g) \rightleftharpoons H_2O(g) + S \quad (1)$$

$$H_2S(g) + \tfrac{3}{2}O_2(g) \rightleftharpoons H_2O(g) + SO_2(g) \quad (2)$$

There are two reasons for the apparent discrepancy between the measured OCV values and the calculated values. The calculated OCV values are based on ideal conditions that do not apply to the practical cell. For example, the equilibrium potential for reaction (2) is expressed by the following Nernst equation (Eq. (3)).

$$\Delta E_N = \Delta E^0(T) - \frac{RT}{6F}\ln\left(\frac{P_{H_2O}P_{SO_2}}{P_{H_2S}P_{O_2}{}^{3/2}}\right) \quad (3)$$

where $\Delta E^0(T)$ is the cell potential calculated from thermodynamic data ΔG^0, i.e. the potential when the partial pressures of all reactants and products are 1 atm. However, in the experiment at 800°C under open circuit conditions, P_{H_2S} was 0.05 atm and P_{O_2} was 0.21 atm. The equilibrium partial pressures of SO_2 and water vapor in the anode compartment were very low at open circuit condition, because the electrochemical exchange current density (i_o) of Eq. (2) was low [2] and the feed gases were "extra dry" grade. If it is assumed that the concentrations of water vapor and sulfur dioxide are each less than 10 ppm in the anode chamber, the calculated equilibrium potential ΔE_N (Eq. (3)) will be 1.023 V at 800°C. This value is in good agreement with the high experimental OCV values.

A second effect that may also contribute to the apparently high values for the OCV is the presence of hydrogen. Trace amounts of hydrogen in the anode chamber have been detected by GC analysis. Under equilibrium conditions, 8.6% of H_2S is thermally decomposed at 827°C (Eq. (4)) [5]. Platinum surfaces are known to catalyze decomposition of H_2S. Competitive electro-oxidation of hydrogen will also occur on the Pt anode (Eq. (5)); the cell reaction is shown in Eq. (6).

$$H_2S(g) \rightleftharpoons S + H_2(g) \quad (4)$$

$$H_2 \rightleftharpoons 2H^+ + 2e^- \quad (5)$$

$$H_2 + \tfrac{1}{2}O_2 \rightleftharpoons H_2O \quad (\Delta E^0 = 0.98\,\text{V, at } 800^\circ\text{C}) \quad (6)$$

The thermal equilibrium potential of hydrogen oxidation (Eq. (6)) is higher than that for H_2S oxidation. Thus, the measured OCV value may be a mixed reaction voltage, the value of which depends on the proportions of each electroactive species present and the reaction potentials. Therefore, the high potential of the hydrogen electro-oxidation reaction would make the measured OCVs of H_2S–O_2 fuel cell higher than theoretical values for H_2S oxidation alone.

The detection of H_2 in the anode gases and the agreement between the calculated and experimental values for the OCV strongly indicate that both factors contribute to the values obtained. The low levels of H_2 detected suggest that the primary mechanism is electrochemical conversion of H_2S, and that thermal decomposition of H_2S to H_2 is a minor parallel mechanism.

3.2. Voltage–current performance and output power density

Fig. 2 shows i as a function of each of cell voltage and power density for the H_2S–O_2 SOFC, 5% H_2S,Pt/$(ZrO_2)_{0.92}(Y_2O_3)_{0.08}$/Pt, air, at 750 and 800°C. The i increases very slowly with reduction in cell voltage above 0.8 V. The i then quasilinearly increases with decrease in potential generated. There is no slope deviation in the high i region, showing that mass transfer is not a limitation for the system [11]. In the potential range between 0.8 and 0.32 V,

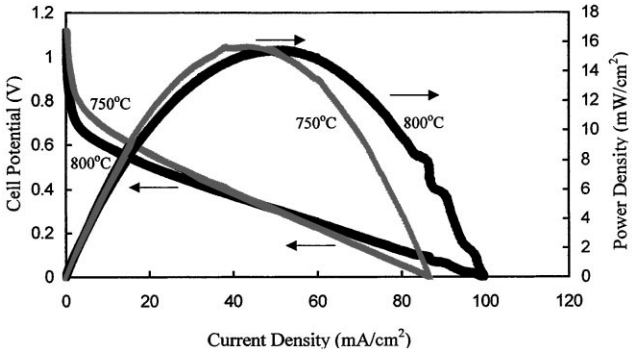

Fig. 2. Performance of 5% H_2S, Pt/8% YSZ/Pt, air fuel cell at 750 and 800°C.

the i at 800°C is unexpectedly lower than that at 750°C. This behavior is abnormal; for most SOFCs the current increases with temperature due to an increase in ionic conductivity of the electrolyte. The cause of this behavior is deterioration of the anode, as will be discussed below. The maximum current densities achieved were 87 mA cm^{-2} at 750°C and 100 mA cm^{-2} at 800°C, respectively. These values are higher than the data for related systems reported to date [2–5]. The superior values obtained using our system when compared with the published data for comparable systems are attributed in part to our use of much thinner self-supporting membranes and good sealing to prevent gas mixing due to crossover. The Pt/YSZ or ceria-based electrolyte/Pt membranes described in the literature [2–5] are typically 0.6–1.5 mm thick, and the low values reported for the open circuit potential indicate that related systems may not have a completely gas-tight seal [4,5].

The maximum power densities attained at the two different temperatures are similar, 15.6 mW cm^{-2} at 750°C and 15.4 mW cm^{-2} at 800°C. The optimum operating values are slightly different. Maximum power density is produced at a i of 44 mA cm^{-2} at 750°C and at 49 mA cm^{-2} at 800°C. Generally, power output is expected to increase with increasing temperature for the same cell configuration [4,12]. The similarity between the maxima is attributed to similar impedance performance at each temperature, as will now be discussed.

3.3. Impedance characteristics

Impedance spectroscopy (IS) of the Pt/YSZ system has been extensively investigated in SOFC studies [13]. Usually, the IS plots comprise two overlapping semicircles. The intercepts of the first high frequency semicircle with the real-axis represent the resistance within YSZ grains and intergranular (grain boundary) resistance. The intercepts for the second semicircle represent the effective resistance for the electrode reaction [13].

Results of H_2S–O_2 fuel cell IS measurements at 750 and 800°C are shown in Figs. 3 and 4. Measurements were made under open circuit conditions (Fig. 3) and polarization

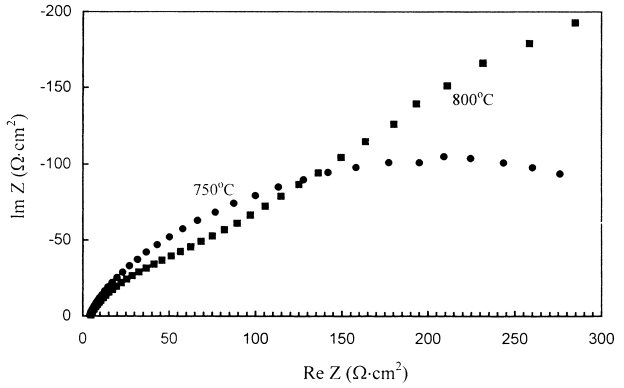

Fig. 3. Impedance spectra of 5% H_2S, Pt/8% YSZ/Pt, air fuel cell at 750 and 800°C under open circuit conditions.

conditions (at 0 V) (Fig. 4). At OCV, the two semicircles evidently are not well developed due to the very high electrode reaction impedance and the lower limit for the frequencies used in the IS test. At 0 V, the two overlapping semicircles are well-defined, as shown by the fit to the simulated curves (Fig. 4). The centers of the semicircles are slightly below the real axis, as a result of either diffusion effects (Warburg impedance) or a distribution of time constants around an ideal value [13].

The first real-axis intercepts (R_1) are the same under both polarization and non-polarization conditions, 4.2 Ω cm^2 at 750°C and 4.6 Ω cm^2 at 800°C. The high-frequency resistance includes the bulk ionic resistance within YSZ grains and the resistance of electrical connection wires. Both types are linear resistance. The resistance due primarily to connecting leads contributes the largest part of R_1, found to be about 2.6 Ω at room temperature. The total resistance of connecting leads increased with operating temperature in part because a section of the platinum wire was heated with the cell in the furnace. As the temperature coefficient of resistance of platinum is 0.00392°C^{-1}, the increase in resistance for 1 m of wire is less than 0.06 Ω from 750 to 800°C. However, the resistance increased by 0.4 Ω when the temperature increased from 750 to 800°C. Therefore, the largest part of increase in the resistance is ascribed to increase in the electronic connection resistance between the Pt wire and Pt anode as well as the contact resistance between Pt anode and the electrolyte. As the data at 800°C were acquired after the *I–V* curve and impedance measurements at 750°C, the long exposure time and pre-polarization of the cell in H_2S stream resulted in the formation of PtS, and consequently increased the electronic connection resistance at 800°C. This interpretation is supported by results from experiments in which the cell was cycled between 750 and 800°C, to be described below.

The grain boundary resistance ($R_2 - R_1$) and electrode reaction resistance ($R_3 - R_2'$) were determined under polarization conditions (at 0 V) (Fig. 4). The intergranular resistance was 3.5 Ω at 750°C and 2.6 Ω at 800°C; electrode resistance at 0 V was 1.8 Ω at 750°C and 2.2 Ω at 800°C.

The intergranular resistance decreased with increasing temperature due to the improvement in ionic conductivity, similar to the behavior of most H_2–O_2 fuel cells [1]. The higher i observed between 0.32 and 0 V at 800°C (Fig. 2) is due to the lower grain boundary resistance at this temperature.

The contributions from anode and cathode reaction resistances can not be distinguished using the cell configuration without a reference electrode. Consequently, the second semicircle is a composite from both cathode and anode reactions. The electrode reaction resistance at 800°C is higher than that at 750°C, and so is not consistent with the Arrenius relationship. The reaction rates of both oxygen reduction and H_2S oxidation increase with temperature [3,14], due to the decrease of activation energies for each reaction. The increase of reaction resistance observed at 800°C is consistent with deterioration of the platinum anode in the H_2S stream. The electrode reaction resistance changes with the cell polarization conditions. High polarization gives low electrochemical reaction resistance. In this case, the electrode reaction resistance at 0 V (Fig. 4) is much lower than that under open circuit conditions (Fig. 3). The i between 0.8 and 0.32 V is lower at 800°C than at 750°C (Fig. 2), resulting from the higher electrode reaction resistance at 800°C.

Thus, the total voltage drop (800°C) in the H_2S–O_2 fuel cell is attributable to three contributing factors: bulk electrolyte and electrical resistance (IR_1), grain boundary resistance ($I(R_2-R_1)$), and electrode reaction resistance (Fig. 5). The total cell ohmic drop (R_2) represents a large fraction of the voltage drop, especially at high current densities. The quasilinear decrease of the cell voltage with increase in i is a

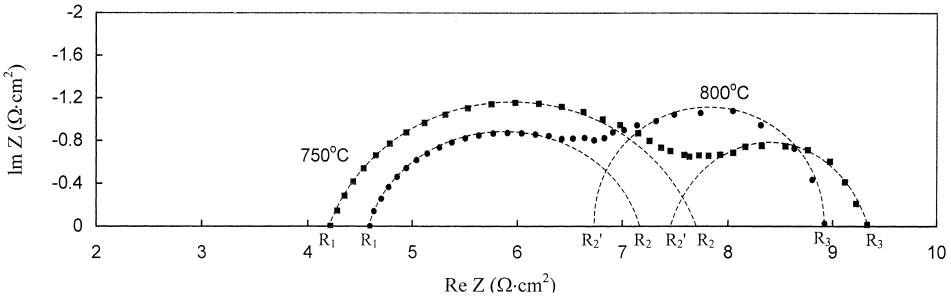

Fig. 4. Impedance spectra of 5% H_2S, Pt/8% YSZ/Pt, air fuel cell at 750 and 800°C at 0 V.

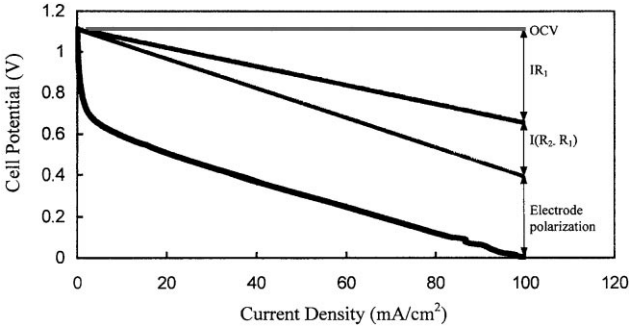

Fig. 5. Contribution of various cell polarization components for a fuel cell at 800°C.

consequence of the large ohmic polarization. The electronic resistance arising from the Pt wires and connections with the Pt anode can be reduced by optimizing the cell design. It is anticipated that the resistance of the electrolyte can be lowered by further reducing its thickness [15]. It is anticipated that further improvements will be realized through development of stable new electrolytes with high ionic conductivity and negligible electronic conductivity, such as improved ceria-based electrolytes [16].

3.4. Effect of feed gas concentration on cell performance

Fig. 6 shows the voltage–current density relationship for use of pure H_2S feed at 750 and 800°C. The cell voltage–current performance at each temperature unexpectedly is worse than that in 5% H_2S feed. The lower maximum i in pure H_2S than in diluted H_2S is attributed to rapid platinum anode deterioration in the concentrated gas stream. It has been found that the platinum anode detaches gradually from the YSZ electrolyte with time on stream. The curvature at the high-current end of the I–V curve at 750°C indicates the beginning of the detachment of the Pt anode. Total lifetime of this cell under polarization condition at 800°C is 6 h, after which time the cell fails. After the test, the Pt anode was found to be completely detached from the electrolyte, while the bonding of the Pt cathode to the electrolyte was intact.

H_2S in the anode feed attacks the Pt surface to form PtS at elevated temperatures, and thereby reduces electrical

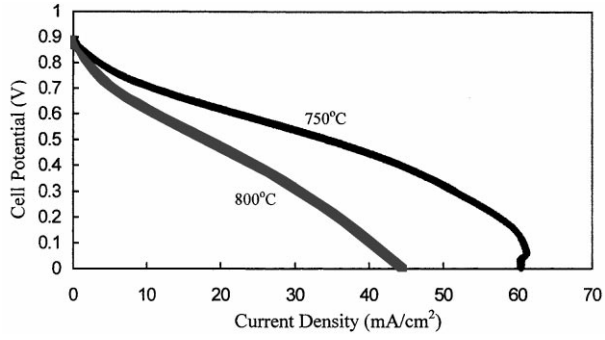

Fig. 6. Current–potential curves of pure H_2S, Pt/8% YSZ/Pt, air fuel cell at 750 and 800°C.

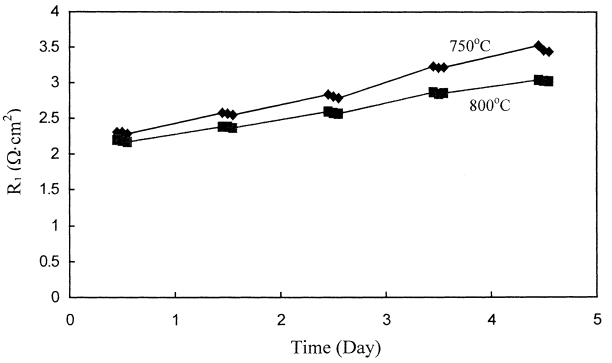

Fig. 7. Resistance (R_1) changes with exposure time under open circuit conditions using pure H_2S feed.

conductivity [17]. Further, the high-frequency resistance (R_1) at different temperatures changes with duration of exposure and polarization time (Figs. 7 and 8). Fig. 7 shows the change in resistance (R_1) with exposure time under open circuit conditions using pure H_2S feed. The temperature of the cell was cycled three times per day between 750 and 800°C, starting at either 750 or 800°C in different experiments. The slight variance in values for R_1 (less than 0.05 Ω) at the same temperature between the three testing times indicates that thermal cycling has no major effect on cell performance. The higher resistance at 750°C compared with 800°C is consistent with the lower ionic conductivity of YSZ membrane at this temperature. During operation over 5 days without polarization, R_1 increased by 1.2 Ω at 750°C, which is attributable to formation of PtS as described above. However, polarization is the primary source of the large increment in the resistance (R_1): about 5.7 Ω in 20 min at high current polarization (Fig. 8). Polarization aggravates the instability of the electrochemical interface between anode and membrane and thus accelerates degradation of the Pt anode.

The impedance spectrum of the membrane assembly using pure H_2S gas under polarization conditions (at 0 V) is shown in Fig. 9. The electrical resistance of the wiring in

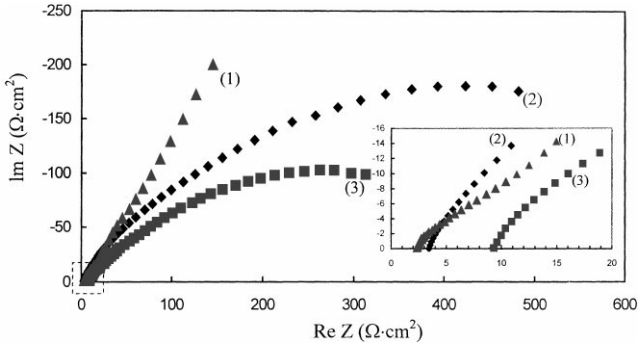

Fig. 8. Impedance spectra of pure H_2S, Pt/8% YSZ/Pt, air fuel cell at 750°C: (1) first day exposure in pure H_2S without polarization; (2) after 5-day operation without polarization; (3) after polarization for 20 min; inset: expanded region 0–20 Ω cm^2.

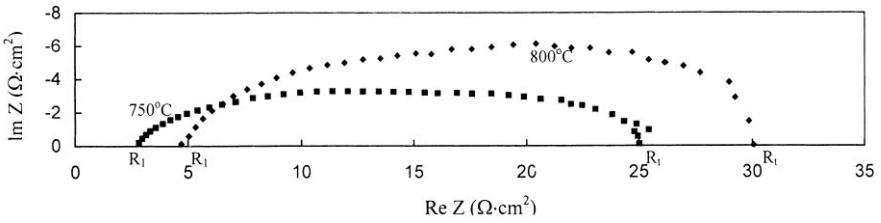

Fig. 9. Impedance spectra of pure H_2S, Pt/8% YSZ/Pt, air fuel cell at 750 and 800°C at 0 V.

this cell is slightly lower than that in the above cell using 5% H_2S as fuel due to the use of shorter connecting wires. Again, the high-frequency resistance of the cell (R_1) increases with temperature: the resistance at 800°C is almost two times larger than at 750°C. In these tests, IS data at 800°C were acquired after the measurements of *I–V* curve and impedance at 750°C. Consequently, the resistance of R_1 has been found to be higher at the higher temperature due to the prior deterioration of the contacts (Fig. 9). Further, the *I–V* relationship (Fig. 6) determined in polarization experiments also shows abnormal behavior: the maximum *i* decreases with increasing temperature.

The IS plots using pure H_2S as feed (Fig. 9) can not easily be deconvoluted into a series of semicircles. However, the total cell resistance (R_t) is readily distinguished at the low frequency intercept for each temperature, and is found to be higher than the corresponding value (R_3 in Fig. 4) for use of 5% H_2S feed. The increase in resistance is consistent with degradation of the Pt anode in the H_2S stream, as discussed above. That is, Pt anode degradation in the pure H_2S stream is more pronounced than in the 5% H_2S stream. The formation of PtS in the Pt/YSZ interface leads to an increase of interface resistance between the Pt anode and YSZ electrolyte. Thus, using pure H_2S adversely affects performance of the H_2S–O_2 fuel cell due to rapid formation of PtS, which has the effects of deactivation of the anode electrocatalyst and increasing the interface resistance.

4. Conclusions

The promising initial values for current and power output using the present system show that hydrogen sulfide is a potentially suitable fuel for a zirconia-based solid electrolyte fuel cell operating at intermediate temperatures (750 and 800°C). However, platinum deposited on YSZ is not a suitable anode material for an H_2S stream. The formation of PtS contaminates the anode surface and increases the interface resistance between Pt and YSZ, ultimately leading to detachment of the Pt anode from the YSZ membrane. Electrochemical polarization accelerates the degradation of the Pt anode significantly. Superior *i* and longer lifetime of the MEA are found when using dilute H_2S feed compared with using pure H_2S feed. Alternative anode catalyst systems are required, that do not deteriorate over time in an atmosphere of H_2S. Electrochemical impedance analysis shows that ohmic drops arising from electrical wire connections, bulk electrolyte resistance and grain boundary resistance each contribute a significant part of the overall cell voltage drop. Shorter electrical wires and reduction of the resistance of connections are both required to improve cell performance.

Acknowledgements

This research has been supported by Natural Sciences and Engineering Research Council of Canada.

References

[1] K. Kordesch, G. Simader, Fuel Cells and Their Applications, VCH Publishers, New York, 1996.
[2] N.U. Pujare, K.W. Semkow, A.F. Sammells, J. Electrochem. Soc. 134 (1987) 2639.
[3] N.U. Pujare, K.J. Tsai, A.F. Sammells, J. Electrochem. Soc. 136 (1989) 3662.
[4] T.J. Kirk, J. Winnick, J. Electrochem. Soc. 140 (1993) 3494.
[5] D. Peterson, J. Winnick, J. Electrochem. Soc. 145 (1998) 1449.
[6] C. Yates, J. Winnick, J. Electrochem. Soc. 146 (1999) 2841.
[7] J. Zaman, A. Chakma, Fuel Process. Technol. 41 (1995) 159.
[8] K.T. Chuang, A.R. Sanger, in: D.H.F. Liu, B.G. Lipták (Eds.), Environmental Engineers' Handbook, Section 5.20, 2nd Edition, Lewis Publishers, Boca Raton, FL, 1997.
[9] S.P.S. Badwal, K. Foger, Mater. Forum 21 (1997) 187.
[10] I.V. Yentekakis, C.G. Vayenas, J. Electrochem. Soc. 136 (1989) 996.
[11] J.O'M. Bockris, S. Srinivasan, Fuel Cells: Their Electrochemistry, McGraw-Hill, New York, 1969 (Chapter 4).
[12] S.J. Visco, L. Wang, S. De Souza, L.C. De Jonghe, Mater. Res. Soc. Symp. Proc. 369 (1998) 683.
[13] J.R. Macdonald, Impedance Spectroscopy: Emphasizing Solid Materials and Systems, Wiley, New York, 1987.
[14] J. Divisek, L.G.J. de Haart, P. Holtappels, T. Lennartz, W. Malléner, U. Stimming, K. Wippermann, J. Power Sources 49 (1994) 257.
[15] T. Tsai, E. Perry, S. Barnett, J. Electrochem. Soc. 144 (1997) L130.
[16] M. Mogensen, N.M. Sammes, G.A. Tompsett, Solid State Ionics 129 (2000) 63.
[17] P. He, M. Liu, J.L. Luo, A.R. Sanger, K.T. Chuang, J. Electrochem. Soc., submitted for publication.